Packaging Technology and Science

WILEY

Packaging Technology and Science
An International Journal

RESEARCH ARTICLE

Flexible Nanobiocomposite Coating Based on Recycled Can Waste as Antimicrobial Active Packaging Materials

Saber Ibrahim[1,2] | Hager Fahmy[3]

[1]Packaging Materials Department, National Research Center, Dokki, Giza, Egypt | [2]Nanomaterials Investigation Lab., Central Laboratory Network, National Research Center, Dokki, Giza, Egypt | [3]Department of Advertising, Printing and Publishing, Faculty of Applied Arts, Benha University, Banha, Qalubia, Egypt

Correspondence: Saber Ibrahim (msa.nrc@gmail.com; sa.ibrahim@nrc.sci.eg)

Received: 13 January 2025 | **Revised:** 27 April 2025 | **Accepted:** 28 April 2025

Keywords: active packaging | Al_2O_3-NPs | nanobiocomposite | paperboard | recycle cans

ABSTRACT

The accumulation of aluminium waste in landfills constitutes a significant environmental challenge due to its substantial presence as solid waste. Conventional disposal and recycling techniques have been employed to mitigate this issue; however, they often result in secondary environmental pollution. In this study, eco-friendly and cost-effective aluminium oxide nanoparticles (Al_2O_3-NPs) were synthesized via a green synthesis approach utilizing date palm seed extract. Flexible polystyrene (FPS) was fabricated through in-situ polymerization in the presence of varying concentrations of Al_2O_3-NPs to develop active nanobiocomposite coatings. The physicochemical characteristics of the synthesized Al_2O_3 nanoparticles were comprehensively analysed using multiple advanced techniques, including dynamic light scattering (DLS), Brunauer–Emmett–Teller (BET) surface area analysis, X-ray diffraction (XRD), scanning electron microscopy (SEM) coupled with energy-dispersive X-ray spectroscopy (EDX) and transmission electron microscopy (TEM). XRD analysis confirmed a rhombohedral crystal structure with an average particle size of 32 nm. Fourier transform infrared spectroscopy (FTIR) and X-ray photoelectron spectroscopy (XPS) further validated the structural composition of the synthesized Al_2O_3 nanoparticles. Additionally, thermogravimetric analysis (TGA) was employed to assess the thermal stability of the FPS/Al_2O_3 bionanocomposite coating, revealing excellent thermal resistance withstanding temperatures $\geq$ 240°C. DLS measurements indicated a uniform particle size distribution with stable zeta potential, while BET analysis demonstrated a substantial surface area ranging between 62 and 147 m^2/g. Furthermore, the antimicrobial efficacy of Al_2O_3 nanoparticles was investigated by determining their minimum inhibitory concentration (MIC) against both Gram-positive and Gram-negative bacteria. The antimicrobial assessment revealed that Gram-negative bacteria exhibited greater resistance compared to Gram-positive bacteria and yeast. Migration analysis demonstrated that the percentage of migrated material was within acceptable limits as per European Commission (EC) regulations. These findings suggest that the developed flexible nanobiocomposite-coated paperboard holds significant potential as an advanced active packaging material.

1 | Introduction

In the field of materials science, polymeric nanobiocomposites represent a promising research domain due to their ability to incorporate inorganic fillers derived from cost-effective waste recycling. These fillers not only enhance the mechanical properties of nanobiocomposites but also exhibit excellent dispersibility within macromolecular matrices [1]. Nanobiocomposite coatings have gained significant attention for their potential applications in various sectors, particularly in active packaging materials [2]. Furthermore, different nanomaterials can exhibit antimicrobial activity when integrated into eco-friendly, water-based coatings through miniemulsion polymerization [3].

Active packaging materials have emerged as an innovative solution in recent years, offering enhanced functionality beyond conventional passive packaging [4]. These materials incorporate active agents that provide antimicrobial properties, extend shelf life and improve product safety [5]. Aluminium oxide nanoparticles (Al_2O_3-NPs), commonly referred to as alumina nanoparticles, are synthesized from aluminium salt precursors or recycled aluminium waste. Aluminium cans, widely used in food and beverage packaging, have been explored as a valuable source for Al_2O_3-NPs through chemical recycling processes [6]. Given their extensive use in metallized packaging, aluminium-based nanoparticles present a sustainable approach for advanced packaging applications [7].

Aluminium nanoparticles can be synthesized using various physical, chemical and biological methods, each offering distinct advantages [8]. Physical techniques such as ball milling and laser ablation involve mechanical force or high-energy laser pulses to reduce bulk aluminium into nanoscale particles. Alternatively, chemical reduction methods utilize aluminium salts (e.g., aluminium chloride) and strong reducing agents such as sodium borohydride, often in the presence of stabilizers to prevent agglomeration. This approach is cost-effective and scalable and allows precise control over nanoparticle size and morphology. Additionally, biological synthesis using plant extracts or microbial agents has gained traction as an environmentally sustainable method, leveraging natural biomolecules for nanoparticle formation [9]. The choice of synthesis technique plays a crucial role in determining nanoparticle properties, including size, morphology and surface reactivity, thereby influencing their applications in catalysis, biomedicine and antimicrobial coatings.

The synthesis method directly impacts the physicochemical characteristics of aluminium nanoparticles, such as stability, dispersibility and reactivity. Physical techniques like laser ablation yield high-purity nanoparticles but require sophisticated instrumentation, while chemical reduction enables controlled size distribution but may introduce impurities from precursor materials [10, 11]. Due to their high reactivity, especially with oxygen, aluminium nanoparticles require protective coatings or stabilizers to prevent oxidation, further influencing their suitability for industrial and biomedical applications.

Several methodologies are available for synthesizing aluminium oxide nanoparticles from recycled packaging cans [12]. A common approach involves controlled oxidation of aluminium metal to form aluminium hydroxide, followed by thermal treatment to convert it into Al_2O_3 nanoparticles. Other techniques, such as sol–gel synthesis, precipitation and hydrothermal processing, can also be employed to achieve high-purity alumina nanoparticles [13]. These nanoparticles exhibit a high surface area-to-volume ratio, excellent thermal and chemical stability and superior biocompatibility, making them ideal candidates for antimicrobial coatings in active packaging applications [14].

To create active packaging materials with antimicrobial properties, aluminium oxide nanoparticles can be incorporated into polymer coatings. These polymer-based coatings act as protective layers, preventing microbial contamination and thereby extending the shelf life of packaged products [15, 16]. Various dispersion techniques, including melt blending, solvent casting and electrospinning, enable the uniform incorporation of Al_2O_3 nanoparticles into polymer matrices [17]. Due to their intrinsic antimicrobial properties, these nanoparticles disrupt microbial cell membranes, leading to inactivation of bacteria and fungi, effectively preventing spoilage and contamination [18].

Active packaging materials containing aluminium oxide nanoparticles offer multiple advantages within the food packaging industry [19]. First, they serve as an additional barrier against microbial contamination, enhancing food safety and maintaining product integrity. Second, these materials contribute to shelf-life extension by inhibiting spoilage-causing microorganisms. Furthermore, aluminium oxide nanoparticles are non-toxic and environmentally friendly, ensuring compliance with food safety regulations and sustainability requirements [20].

The application scope of these active packaging materials is extensive, encompassing food and beverage packaging, pharmaceuticals and healthcare products [21]. By incorporating Al_2O_3 nanoparticles into polymer coatings, manufacturers can develop innovative packaging solutions that enhance product quality, minimize waste and improve consumer safety.

This study aims to integrate nanobiocomposite formulation science with nanoemulsion polymerization techniques to develop a water-based nanobiocomposite coating with superior antimicrobial properties. The research focuses on synthesizing aluminium oxide nanoparticles from recycled packaging cans and incorporating them into polymeric coatings for active packaging applications.

2 | Materials and Methods

2.1 | Materials

Styrene was purified before using. Azo-bis-isobutyronitrile (AIBN), methanol, sodium hydroxide, sodium n-dodecyl sulfate (SDS), calcium hydride, sodium octyl sulfate (SOS), 1-(2-butoxy-1-methylethxy)propane-2-ol (BMEP), sodium chloride and hexadecane (HD) are used as received. Al-cans were collected from the central waste collection of the National Research Centre, Egypt. Thymol extracted from thyme leaves was obtained by solid/liquid extraction method through maceration and Soxhlet processes [22].

2.2 | Green Synthesis of Al_3O_2-NPs

The green synthesis of aluminium oxide nanoparticles (Al_2O_3-NPs) was carried out following the procedure outlined below. In brief, aluminium cans were utilized as the precursor for the biosynthesis of Al_2O_3-NPs. A total of 30 g of aluminium cans was dissolved in 300 mL of 6-M hydrochloric acid under gentle stirring at ambient temperature, leading to the formation of aluminium chloride hexahydrate ($AlCl_3{\cdot}6H_2O$). The resulting supernatant was collected and subjected to centrifugation at 15 000 rpm for 25 min.

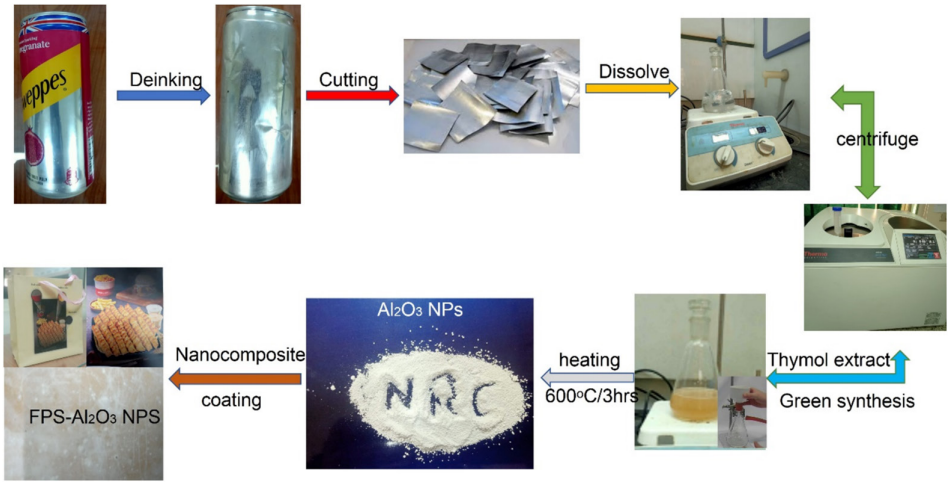

SCHEME 1 | Schematic diagram of FPS-Al_3O_2-NPs green synthesis.

Subsequently, an equal volume ratio of thymol bioactive extract was added to the supernatant under continuous stirring, inducing the formation of a white precipitate. The precipitate was separated by centrifugation and washed four times with Millipore water to remove any residual impurities. The obtained powder was then dried at 80°C for 12 h. Following the drying process, the powder underwent gradual calcination in a muffle furnace at 700°C for 4 h. The final product, Al_2O_3-NPs, was collected, packaged and stored at ambient temperature for further analysis, as illustrated in Scheme 1.

2.3 | Synthesis of Flexible Coating

Flexible polystyrene (FPS) was prepared according to Ibrahim et al. [23] with little modifications. A three-neck flat-bottom flask, a quantified amount of styrene and 0.035 mol of hexadecane were charged with 0.015 mol of SDS, 0.012 mol of SOS and 0.018 mol of BMEP in 0.38 mol of water. Aluminium oxide nanoparticles were charged and emulsified with different ratios. The reactants were degassed for three cycles of (vac/N_2) while stirring for 70 min at 800 rpm. Mini-emulsion was homogenized by ultrasonic for 11 min at 80% amplitude with (Q-Sonica, USA). A stream of N_2 was passed while cooling the emulsion in crash ice water. Afterward, an initiator was charged (0.00192 mol of AIBN in 0.39 mol of degassed water under over 30 min). The reaction was performed at 800 rpm for 4 h, and then the mixture was stirred for 4 h at 800 rpm and cooled until room temperature. FPS/Al_2O_3 NPs were precipitated in methanol under stirring to remove all residual SDS and AIBN in filtrate, and the powder was dried at 60°C in a vacuum oven overnight. Flexible nanocomposites' powder coating was redispersed in water to be applied as a nanobiocomposite coating for prepared paperboard.

2.4 | Coating of Paper Sheet

Paperboard with 180 g/m^3 was used as substrate to apply FPS coating through automatic film coater model GN-VC 10H, China. Coating was carried out at speed of 10 m/s and dried under vacuum of 0.1 mbar at 40°C according to Ibrahim et al. [3].

2.5 | Characterization Techniques

2.5.1 | Particle Size and Zeta Potential

Mean diameter of the nano-FPS particles was measured by dynamic light scattering (DLS) (NICOMP 380 ZLS, PSS, Santa Barbara, CA, USA). In addition, the zeta potentials of the emulsion samples were determined at 18°.

2.5.2 | Surface Area Measurement

Nitrogen ads./des. measurements were carried out by Nova Touch LX4 Quantachrome, USA, to determine complete isothermal parameters. The pore volume was taken from the adsorption branch of the isotherm at $P/P_o = 0.995$, assuming complete surface saturation.

2.5.3 | Total Heavy Metals Determination

Prior to metal determination, all samples were digested using nitric acid. The heavy metals were performed on the Agilent 5100 Inductively Coupled Plasma–Optical Emission Spectrometer (ICP-OES) with Synchronous Vertical Dual View (SVDV).

2.5.4 | Overall Migration

The overall migration (OM) simulants and conditions are detailed in EU Regulation Nr. 10/2011. All samples were compared to a blank sample, and the overall migration is expressed as the amount in milligrams of residual from 1 dm^2 (mg/dm^2). Overall migration results were calculated according to EN 1186-5-single side contact in cell test.

2.5.5 | Toxicity Test

Toxicity test was carried out by using Microtox analyser 500. EC50% is the effective concentration causing 50% of

luminescence inhibition. Origin of the bacteria: Marine luminescent bacteria *Vibrio fischeri*.

2.5.6 | Investigation of Morphological Structure

A Quanta 400F SEM combined with EDX was used to investigate the morphology of the coatings. In addition, TEM was used to investigate FPS and nanobiocomposite materials by JEOL 120/JEOL 200 TEM (Carl Zeiss NTS) operated at 120 kV/200 kV.

2.5.7 | FTIR Spectroscopy

The FT-IR studies have been recorded on a Bruker Alpha II Spectrometer, Germany, with the KBr pellet method in the range of 400–4000 cm^{-1}.

2.5.8 | TGA

The thermal behaviours of FPS/Al_2O_3 nanobiocomposites were analysed through thermogravimetric analysis (TGA; Q50, TA Instruments, Newcastle, Delaware, USA). An average of 10 mg of each sample was heated to 1000°C at a rate of 10°C/min. The TGA measurements were carried out under a nitrogen atmosphere.

2.5.9 | XPS

XPS was collected on K-ALPHA (Themo Fisher Scientific, USA) with monochromatic X-ray Al K-alpha radiation –10 to 1350 eV spot size 400 μm at pressure 10^{-9} mbar with full spectrum pass energy 200 eV and at narrow spectrum 50 eV.

2.5.10 | X-Ray Diffraction (XRD) Analysis

A fine powder of the studied samples was used for X-ray diffraction (XRD) measurements. The data were collected at ambient temperature using a computer-controlled X-ray diffractometer (PAN analytical Empyrean) with Cu Kα radiation (k ka51.5406 A°) operated at 30 mA and 45 kV.

2.5.11 | Study of Printed Nano Coated Paperboard

The design of the packaging bag was constructed in the Adobe Illustrator CC 2018 program in cyan, magenta, yellow and black (CMYK) colours. The packaging bag was printed on 200 g/m^2 craft sheet (210 × 297 mm) using a printing press, the Heidelberg offset machine SM52 MODEL 2003. The colour quality of printed items was measured for the design of the packaging bag by X-Rite exact TM spectrophotometer.

The printing properties were evaluated according to measurement of the rate of change for red, yellow and orange as a group of printing colours. The effect of ageing thermal ink on craft material was applied according to ASTM F1980 and compared the colour character before and after ageing by X-Rite exact TM spectrophotometer.

2.5.12 | Mechanical Properties

Mechanical properties of casted films, tensile strength (TS) and elongation at break (E) of films were measured by Zwick/RoellZ020 instruments (Ulm, Germany) according to ASTM-D412.

2.5.13 | Antimicrobial Activity

The facility of the tested material to decrease the microbial growth was investigated against the standard pathogen strains, Gram-negative bacteria (*Pseudomonas aeruginosa*), Gram-positive bacteria (*Staphylococcus aureus*), unicellular fungi (*Candida albicans*) and multicellular fungi (*Aspergillus niger*). In addition, the evaluation of tested materials to inhibit the microbial proliferation was assessed based on the inhibition zone diameter (mm)/piece.

3 | Results and Discussion

3.1 | Characterization Techniques

3.1.1 | Particle Size

The intensity-weighted Gaussian distribution of particle size for FPS, Al_2O_3-NPs and various polymer composite formulations is presented in Figure 1. The unimodal, homogeneous particle size distributions indicate a uniform dispersion of nanoparticles within the polymer matrix [24]. Furthermore, the FPS/Al_2O_3 nanobiocomposite coatings exhibited effective dispersion of inorganic nanoparticles within the organic polymer matrix at low concentrations. FPS/Al (1%) displayed a particle size of 375 nm with a polydispersity index of 0.75, indicating an optimal particle size distribution, as shown in Figure 1. However, increasing the concentration of inorganic nanoparticles within the nanobiocomposite coatings resulted in a corresponding increase in mean particle size, reaching 821 and 980 nm for Al_2O_3-NPs at 3% and 5% loading, respectively. Consequently, the particle size distribution deviated from the typical bell-shaped curve, reflecting the impact of higher nanoparticle concentrations on aggregation and dispersion behaviour.

The particle size distribution (PSD) of dispersed particles in an emulsion coating significantly influences its properties, including stability, appearance and application characteristics. A narrow PSD with uniform particle size enhances emulsion stability by reducing the tendency of smaller particles to diffuse into larger ones according to Ostwald ripening [25]. Smaller particles promote better coalescence, resulting in smoother films with lower porosity. Smaller particles scatter light less, contributing to higher gloss and transparency [26]. A well-controlled PSD contributes to better mechanical strength by ensuring uniform stress distribution in the film. Finer particles increase surface area, accelerating solvent evaporation and reducing drying time [27]. Overall, optimizing particle size distribution is crucial for achieving desired performance in emulsion coatings, balancing stability, application properties and final film characteristics. According to previous research works, diversion of particle size in a range of 300–350 nm with narrow distribution and excellent uniform

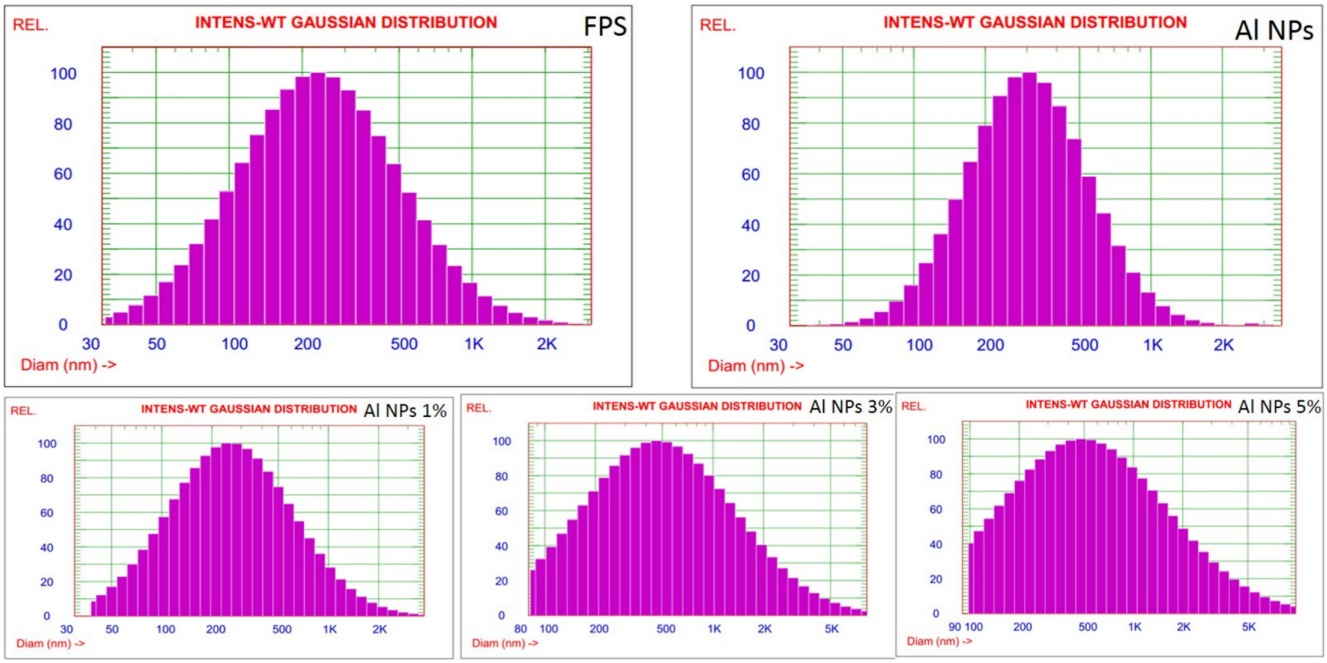

FIGURE 1 | The particle size distribution of FPS, Al_2O_3-NPs and different ratios in polymer composites.

small particle size enhanced better coalescence, higher gloss and transparency, accelerated solvent evaporation and reduced drying time as a very good active coating.

3.1.2 | Zeta Potential

The charge over the dispersed particles is playing a unique character, especially the degree of stability during ageing. Zeta potential of FPS, Al_2O_3-NPs and nanobiocomposites ratios were measured in an aqueous medium at low voltage for semitransparent dispersed samples. The average zeta potentials were present in the range of -11 ± 0.32 and -32 ± 0.53 mV for FPS and Al_2O_3-NPs as the two main components for nanobiocomposites. The three prepared nanobiocomposites coated with various ratios from 1% up to 5% exhibited zeta values in between the measured lines for FPS and Al_2O_3-NPs, as shown in Figure 2. The average zeta potentials of coating nanobiocomposites are -22.3 ± 0.21, -22.4 ± 0.23 and -28.8 ± 0.24 for sequence ratios of 1%, 3% and 5% of FPS/Al_2O_3-NPs, respectively. These findings indicate that dispersed polymer nanobiocomposites coatings were stable at all ratios [28].

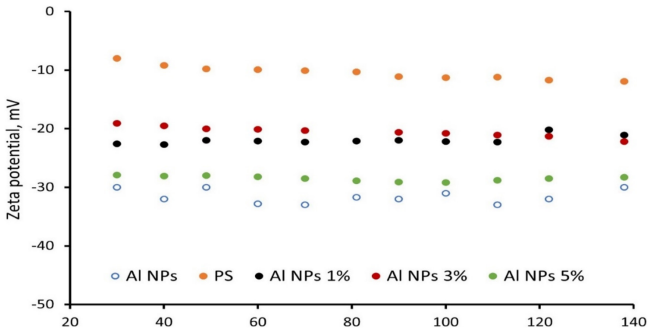

FIGURE 2 | Zeta potential of FPS, Al_2O_3-NPs and different ratios in polymer nanocomposites.

3.1.3 | Surface Area

Measurement of surface area through an isothermal gas adsorption/desorption process is one of the most accurate techniques. The effective calculation of BET for nanobiocomposite coatings was nitrogen gas adsorption in monolayer adsorption in the P/P_o range of 0.05 to 0.30 [29]. Surface areas and relative indices for FPS, Al_2O_3-NPs and different ratios of nanobiocomposite coatings were tabulated in Table 1. Surface areas of FPS and Al-NPs were ≈148 and 137 cm^2/g, respectively, which indicated nice surficial activity for nanopolymer and inorganic materials. Additionally, the nanobiocomposites exhibit decreasing surface areas by increasing the ratio from 1%, 3% to 5% by 103, 70 and 62 cm^2/g, respectively. The previous results have a great agreement and confirmation with the particle size measurements according to the known inverse proportion between particle size and surface area [30].

3.1.4 | SEM–EDX Analysis

Figure 3 illustrates the SEM photograph of Al_2O_3-NPs at different magnifications (×10 k and ×20 k). The topographic morphology represents primary particles in a rocks shape. The main structure of the produced nanoparticles shows little variation in Figure 3. The particles are loosely aggregated, resulting in a porous powder form. The principal particles are in a nano form with variable grades of aggregation, which is a characteristic result of the green preparation method [31]. Figure 3 presents the EDX-mapping results for Al_2O_3-NPs.

TABLE 1 | Surface area of FPS, Al-NPs and different ratios in polymer composites.

Sample	Isotherm branch	Slop	Intercept	Correlation coeff. (*R*)	Surface area (cm^2/g)
FPS	Adsorption	9.477	35.267	0.9995	147.8
Al-NPs		25.256	0.2416	0.9999	136.6
AL-NPs 1%		11.486	22.409	0.8365	102.7
AL-NPs 3%		13.572	36.144	0.7351	70.0
AL-NPs 5%		18.626	37.474	0.8128	62.1

The elemental mapping results indicate the presence of Al and O elements, confirming the composition as Al_2O_3-NPs. The spreading of both Al and O on the sample is random and consistent. Additionally, Figure 2c shows the corresponding energy dispersive X-ray spectroscopy (EDX) elemental analysis results as shown in Figure 3.

3.1.5 | TEM Analysis

TEM images in Figure 4 were stipulated as a visual representation of the morphology of Al_2O_3-NPs. The nanoparticles are spread over a range of particle sizes and possess a defined structure with some clustered nature. The images also indicate that the prepared nanoparticles remain less agglomerated and have uniformly sized particles [32]. Figure 4 shows the XRD pattern, which confirms the rhombohedral phase of Al_2O_3-NPs. Figure 4 illustrates the diffraction pattern (SAED) of Al_2O_3-NPs, which reveals a polycrystalline nature. The d-spacing values obtained from the SAED pattern are in accordance with the reported XRD data.

3.1.6 | XRD Analysis

The peaks resulting from X-ray diffraction of the prepared aluminium oxide nanoparticles are shown in Figure 5. Analysis of the powder XRD pattern of 2θ-Al_2O_3-NPs exposed diffraction peaks at 25.490°, 35.032°, 37.663°, 43.207°, 52.391°, 57.302°, 66.290°, 68.048° and 76.752°, which correspond to hkl planes (012), (104), (110), (113), (024), (116), (214), (300) and (1010) respectively. The hkl planes confirmed the formation of Al_2O_3-NPs with a rhombohedral axes, which fit the R-3c (167) space group. The detected lattice relative intensities and parameters of the diffraction peaks were matched closely with JCPDS PDF Card No: 87-0711. Furthermore, the outcomes are reliable with previously reported results.

3.1.7 | FTIR Spectroscopic Study

Figure 6 represents the FT-IR spectrum of the product recorded to define the vibrational frequency of metal–oxygen present in the α-Al_2O_3 nanoparticles. No impurities or moisture peaks corresponding to the organic matter and/or water were observed. However, the peak at 829 cm^{-1} in the FTIR spectrum of Al_2O_3 is typically associated with Al-O vibrations, particularly related to Al-OH bending or lattice vibrations in alumina structures. Strong absorption bands at 563 cm^{-1} can be assigned to the stretching vibration of the Al-O bond [33].

3.1.8 | XPS

X-ray Photoelectron Spectroscopy (XPS) is a powerful surface analysis technique used to determine the elemental composition, chemical state, and electronic structure of materials. The provided spectra correspond to an analysis of aluminium oxide (Al_2O_3), showing core-level peaks for oxygen (O 1s), carbon (C 1s) and aluminium (Al 2p) as shown in Figure 7.

The survey spectrum displays a broad energy range (0–1200 eV) and provides an overview of the elements present on the surface. The prominent peaks in the spectrum include O 1s (~532 eV) that represents the oxygen component in the Al_2O_3 film, C 1s (~285 eV) expected due to adventitious carbon contamination from exposure to the atmosphere and Al 2p (~74 eV), corresponding to aluminium in the Al_2O_3 matrix. The intensity of the peaks points to the fact that oxygen and aluminium are the dominant elements, confirming the presence of an Al_2O_3 layer [34].

The high-resolution O 1s spectrum is deconvoluted into multiple peaks, indicating the presence of different oxygen species. The main peak at ~532 eV corresponds to lattice oxygen (O^{2-}) in Al_2O_3. The residual plot shows the quality of peak fitting, with minimal deviation, confirming the accuracy of the deconvolution process.

The C 1s spectrum is often included to account for surface contamination. It is deconvoluted into multiple components at ~285 eV, which represent adventitious carbon (C-C, C-H bonds). In addition, at ~286–288 eV, it is assignable to C-O and C=O functional groups, likely due to atmospheric exposure. The presence of carbon does not influence the Al_2O_3 composition but should be considered when interpreting oxygen-related peaks.

The Al 2p spectrum shows a primary peak at ~74 eV, which is characteristic of Al^{3+} in Al_2O_3. Deconvolution reveals at least two components (Scans A and B), possibly due to variations in oxidation states or surface hydroxylation. The residuals indicate a good fit, confirming that aluminium is in its oxidized state, with no significant presence of metallic aluminium (which would appear at lower binding energies, ~72 eV) [35].

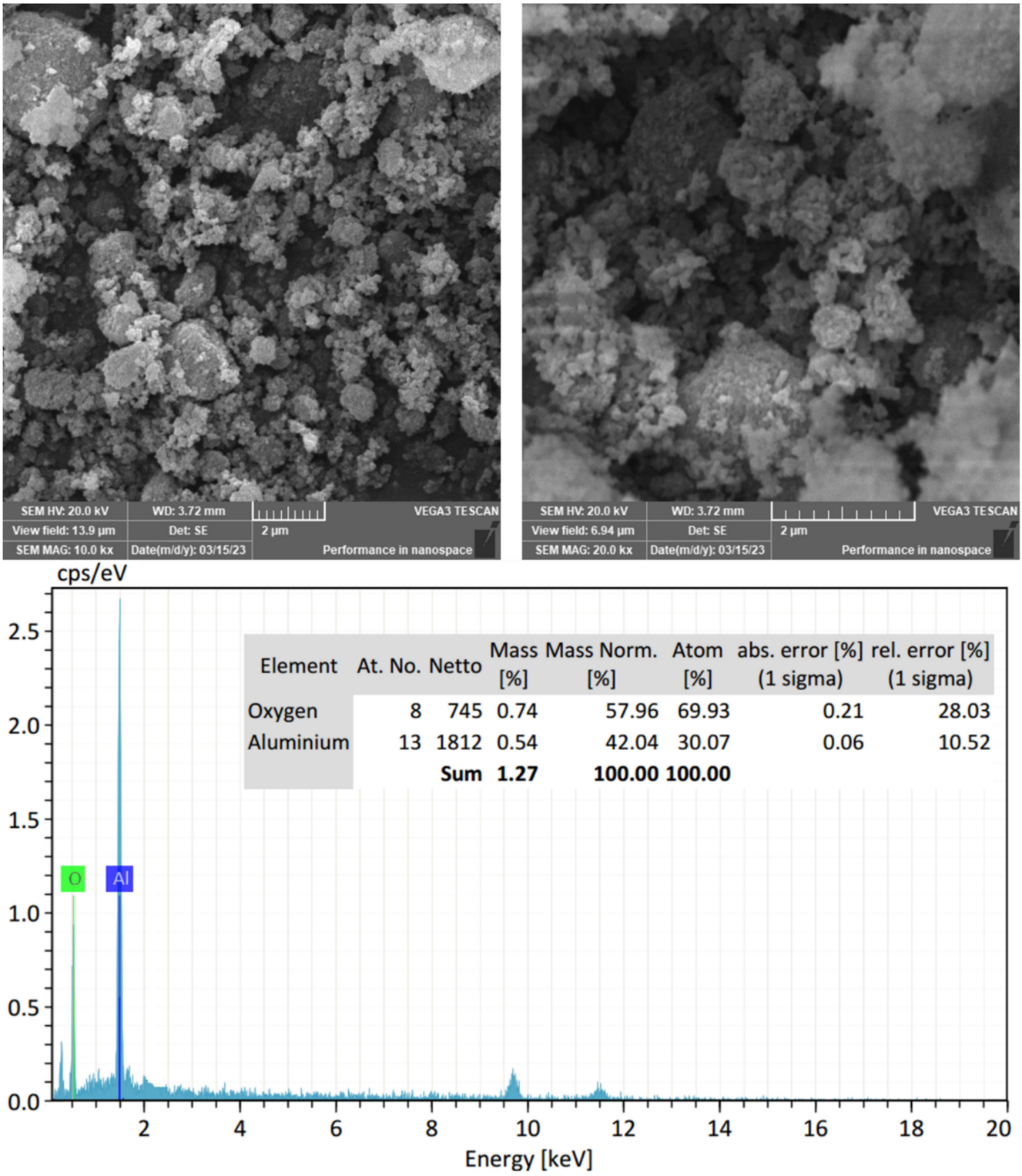

FIGURE 3 | SEM spectrum and EDX results for synthesized Al_2O_3-NPs: SEM spectrum and EDX spectrum.

3.1.9 | TGA

Thermogravimetric Analysis (TGA) is a key technique used to study the thermal stability and decomposition behaviour of materials. It measures the weight change of a sample as a function of temperature or time under a controlled atmosphere. For flexible polystyrene/aluminium oxide nanoparticles synthesized via green synthesis, TGA provides insights into the thermal stability, organic content, and possible phase transitions.

As shown in Figure 8, The graph consists of multiple TGA curves, each representing a different composition of FPS/Al_2O_3 nanoparticles. The TGA curve in the image depicts the weight percentage as a function of temperature, ranging from

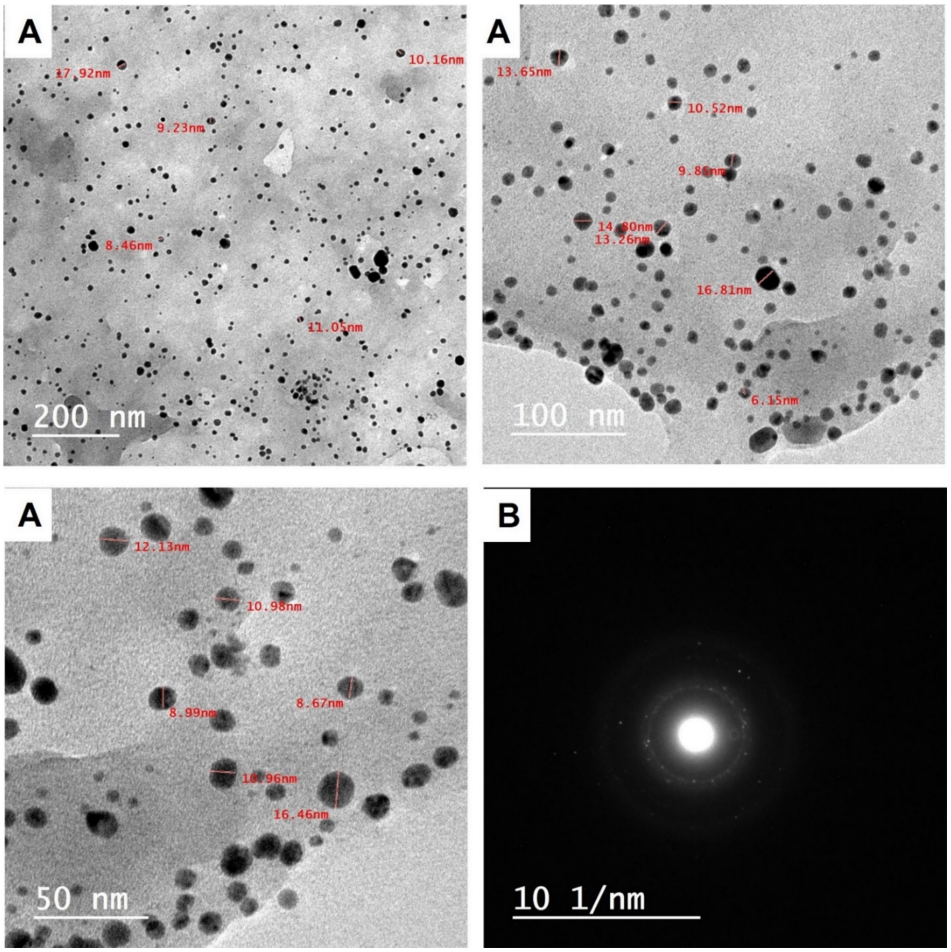

FIGURE 4 | HR-TEM analysis of Al_2O_3-NPs (a) and SAED pattern of Al_2O_3-NPs (b).

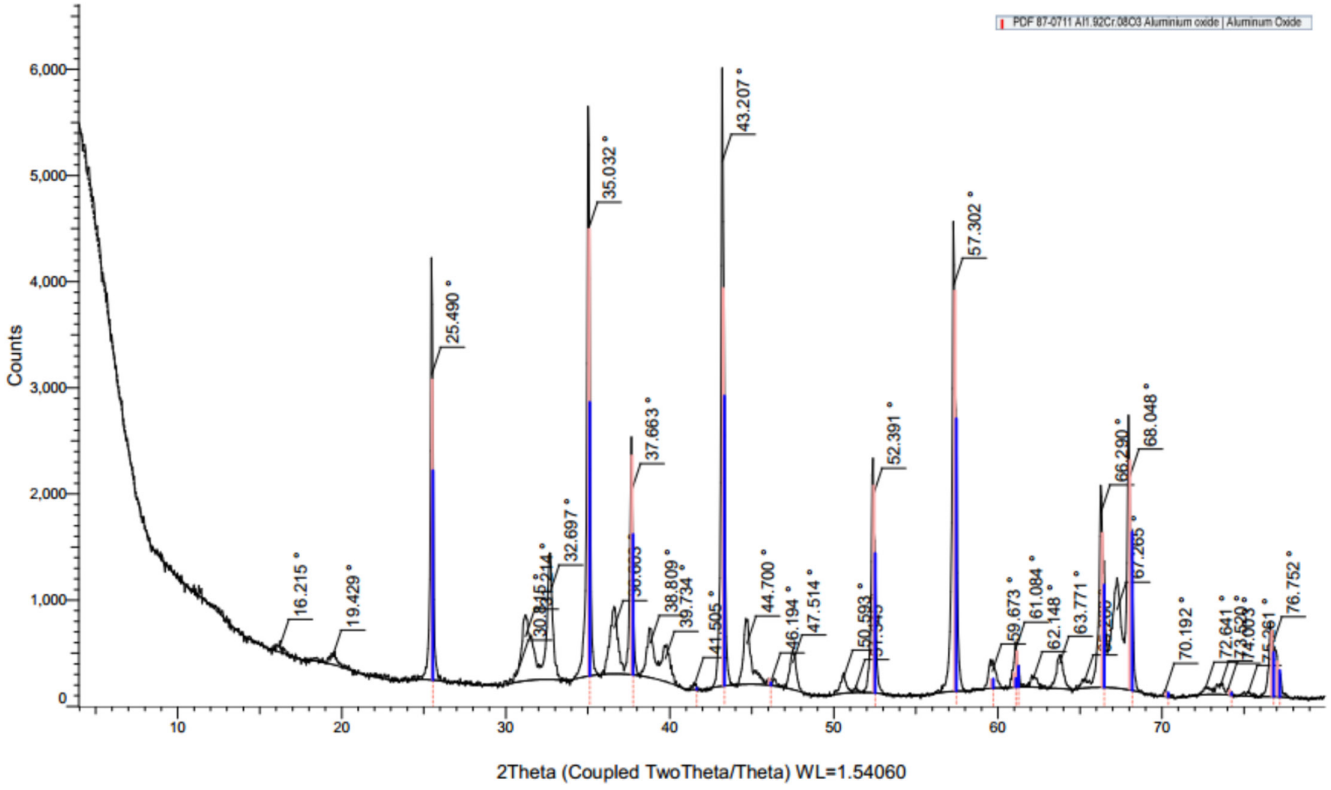

FIGURE 5 | XRD patterns of Al_2O_3 nanoparticles.

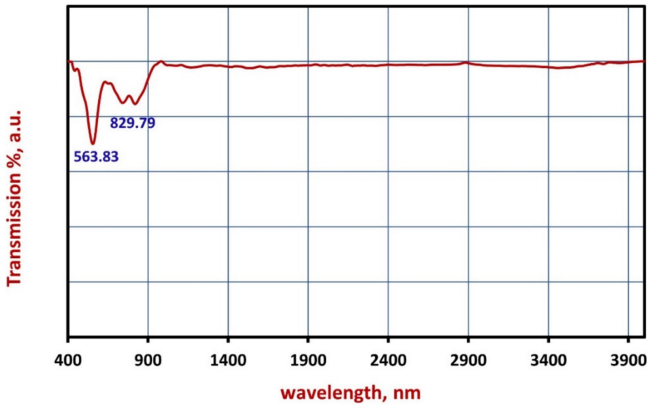

FIGURE 6 | Illustrated FTIR spectrum of Al_2O_3 nanoparticles.

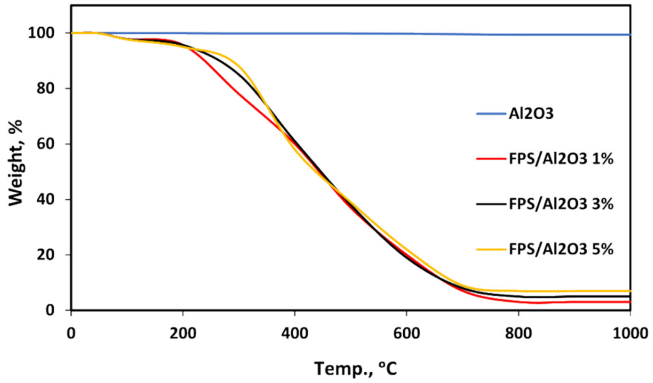

FIGURE 8 | Illustrated TGA of FPS/Al_2O_3 nanoparticles with different ratios.

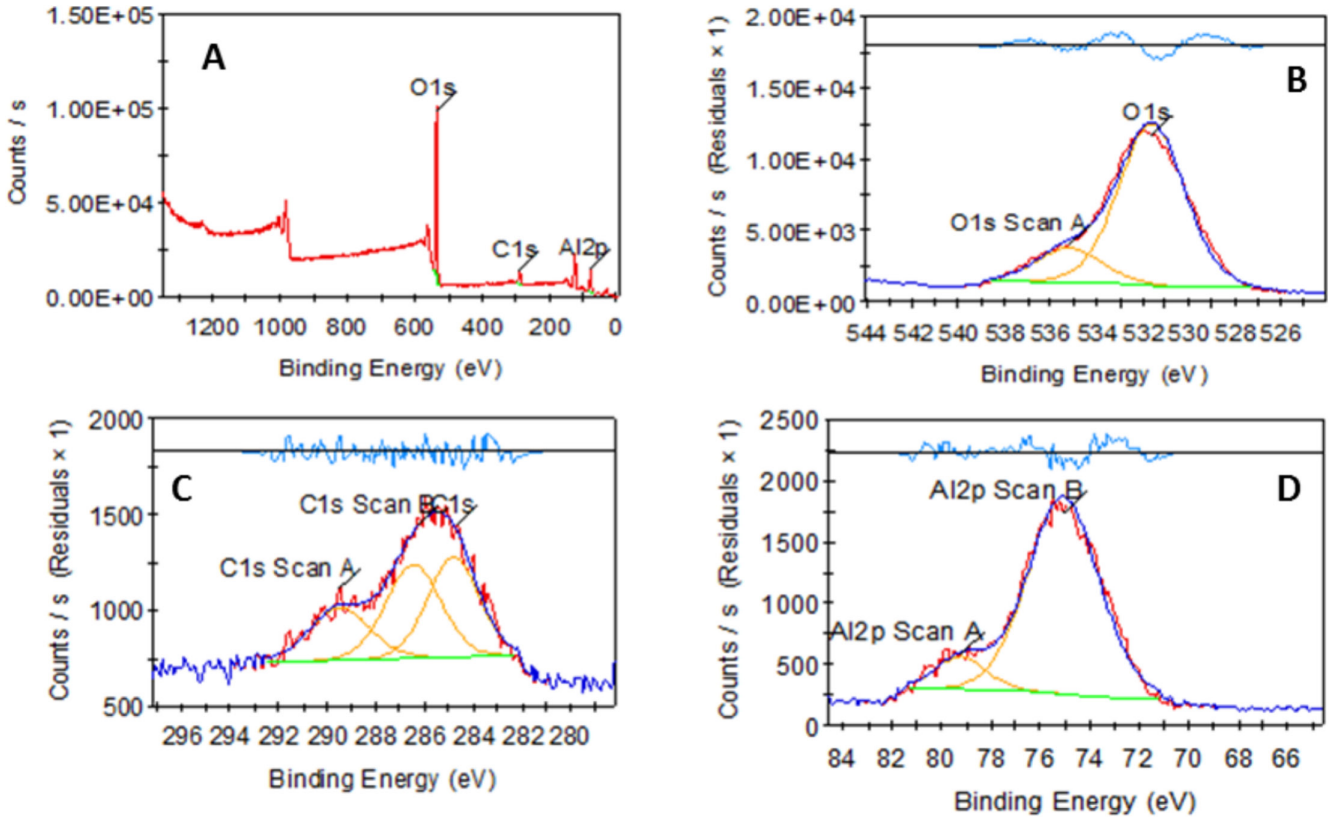

FIGURE 7 | Illustrated XPS bands of Al_2O_3 nanoparticles: (A) survey spectrum, (B) O1s, (C) C 1s and (D) Al 2p deconvolutions.

approximately RT to 1000°C. Al_2O_3 NPs thermograph remains almost constant across the entire temperature range, indicating that FPS alone is highly thermally stable and does not undergo significant degradation. The minimal weight loss indicates that Al_2O_3 nanoparticles are highly stable at elevated temperatures, making them suitable for high-temperature applications such as catalysts, ceramics and coatings [36]. For FPS with lower Al_2O_3 ratio, 1% shown mass loss begins at a lower temperature compared to FPS alone, suggesting that the addition of Al_2O_3 nanoparticles at a lower ratio influences the decomposition process. A sharper decrease in weight percentage indicates that the presence of Al_2O_3 promotes thermal degradation to some extent. The decomposition of FPS/Al_2O_3 5% starts at a slightly higher temperature compared to the red curve, implying that an increased Al_2O_3 content enhances thermal stability. However, the overall weight loss is more gradual, indicating that a higher concentration of Al_2O_3 nanoparticles leads to improved heat resistance. The TGA analysis demonstrates that increasing the Al_2O_3 nanoparticle ratio improves the thermal stability of FPS.

3.1.10 | Antimicrobial Evaluation

As shown in Figure 9, the tested materials with different concentrations had a strong antibacterial activity; however, all

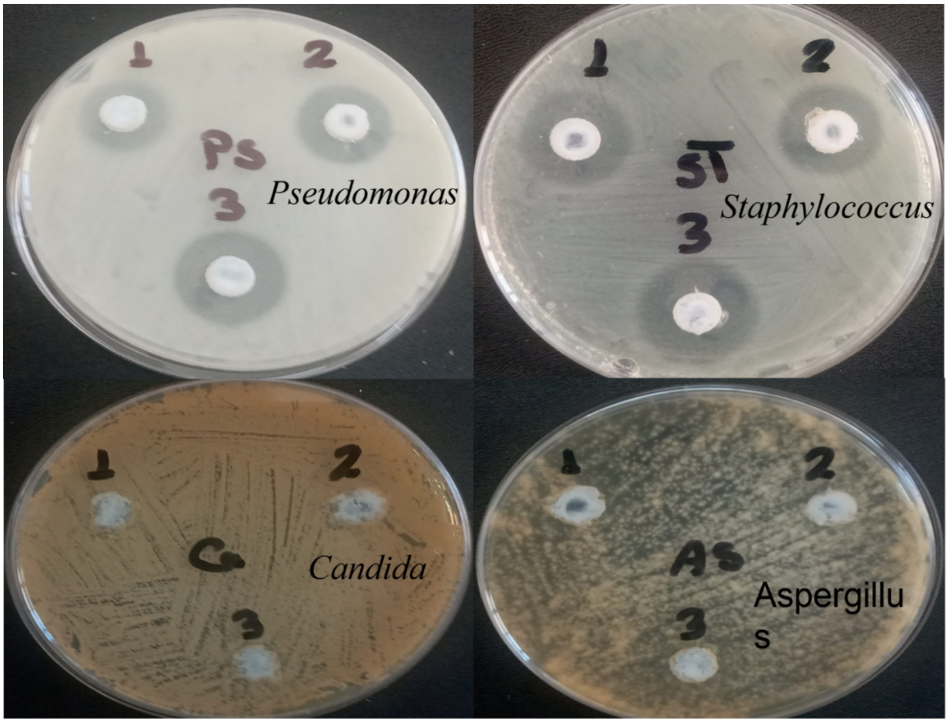

FIGURE 9 | Antimicrobial activity expressed as halo zones of the prepared nanobiocomposite coating loaded with different concentrations of Al_2O_3-NPs against four pathogenic microbes.

TABLE 2 | The overall migration of FPS/Al_2O_3 nanobiocomposites.

	EN-1186-5 Migration into 10% v/v ethanol (Simulant A) mg/dm²			*EN-1186-5* Migration into 20% v/v ethanol (Simulant B) mg/dm²			*EN-1186-5* Migration into 3% w/v acetic acid (Simulant C) mg/dm²			*EN-1186-4* Migration into olive oil (Simulant D_2) mg/dm²		
Replicates	**1%**	**3%**	**5%**	**1%**	**3%**	**5%**	**1%**	**3%**	**5%**	**1%**	**3%**	**5%**
1	2.1	2.5	2.8	3.4	3.5	4.1	4.2	4.6	4.7	0.1	0.1	0.1
2	2.4	2.6	2.7	3.5	3.7	3.9	4.3	4.9	4.9	0.1	0.1	0.1
3	2.2	2.7	2.9	3.6	3.9	3.8	4.1	4.8	5.1	0.1	0.1	0.1
Mean	**2.3**	**2.6**	**2.8**	**3.5**	**3.7**	**3.9**	**4.2**	**4.8**	**4.9**	**0.1**	**0.1**	**0.1**
Limit		**10.0**			**10.0**			**10.0**			**10.0**	

fungal pathogens were able to proliferate in the presence of the tested material, which reflected there was no found inhibition activity of the tested material towards the tested fungal strains. Therefore, the tested material was proved to be an antibacterial agent only [37, 38].

3.1.11 | OM and Toxicity Tests of Coated Paperboard

One of the vital characteristics for any prospective packaging materials is evolution of the migrated substance from packaging film to packaged items. For that, the overall migration test was applied to prepared nanobiocomposite films according to EC 10/2011. According to the coating application on a paperboard substrate, the migration test was applied with two simulants (water and 20% ethanol). The migrated values of substances from bulk films to one-side contact simulants are presented in Table 2. The water simulant was extracted with 20% ethanol and 3% acetic acid at concentrations ranging from 3.5 to 3.9 and 4.2 to 4.9 mg/dm², respectively. All determined migrated values were under the acceptable limit according to the EC 10/2011 standard. These results give a strong recommendation to apply prepared packaging materials (paperboard coated with nanobiocomposites) in food-contact applications.

In addition, the modified flexible polystyrene-coated paperboard shows the effective concentration causing 50% of luminescence inhibition, $EC_{50}\% \geq 100$ at pH 7.4. This is pointed to a safe behaviour of coated packaging material as non-toxic character in contact with packing items.

TABLE 3 | Detection limit of migrated heavy metals of FPS/Al_2O_3 nanobiocomposites.

	Metal	Technique used	Unit	Results		
				1%	3%	5%
1	**Hg**	ICP-OES	ppm	≤ 0.05	≤ 0.05	≤ 0.05
2	**Cd**	ICP-OES	ppm	≤ 0.05	≤ 0.05	≤ 0.05
3	**Cr**	ICP-OES	ppm	≤ 0.05	≤ 0.05	≤ 0.05
4	**As**	ICP-OES	ppm	≤ 0.05	≤ 0.05	≤ 0.05
5	**Pb**	ICP-OES	ppm	≤ 0.05	≤ 0.05	≤ 0.05

FIGURE 10 | Printed design of coated paperboard bag.

TABLE 4 | Printing parameters of design on the paperboard.

Sample	Design after ageing	The original design	Colour change
LAB			
A	l 30.95	l 28.23	(ΔE) E 3.62
	a 30.47	a 28.21	
	b 16.25	b 17.10	
B	l 54.18	l 54.06	(ΔE) E 3.77
	a 17.02	a 17.62	
	b 38.46	b 47.73	
C	l 40.28	l 39.97	(ΔE) E 4.13
	a 31.68	a 33.22	
	b 32.82	b 35.57	
Density			
A	1.52	1.61	D 0.09
B	1.31	1.43	D 0.12
C	1.52	1.64	D 0.08

3.1.12 | Heavy Metals Detection

Table 3 contained the results of heavy metal measurements through ICP plasma. Tabulated results indicated an undetectable concentration of five heavy metals (mercury, cadmium, chrome, arsenic and lead) under the detectable limit of the instrument. This points to the safety of using our nanocomposite coating in food packaging applications as active coating material.

3.1.13 | Printing Properties of Packaging Items

The next table shows the rate of colour change (ΔE) in the selected measured places within the after and before ageing samples (printed design of coated paperboard bag as shown in Figure 10) within the allowable limits according to ISO 12647. The results show that the color change (A Δ3.62), (B Δ3.77) and (C Δ4.13) is in an acceptable range of color variation for printing materials.

The measured densities of the printed craft sheet illustrated small variation between before and after ageing printed sheets, as shown in Table 4. The intensity of (A) red colour, (B) yellow colour and (C) black colour was shifted by 10%, 12% and 12%, respectively. The result has good agreement with previous literature research work [39].

From the previous set of measurements, the printed paper board sheets are not affected by ageing, thus attracting the customer and preserving the bag shape without causing curling.

4 | Conclusion

The synthesis of aluminium oxide nanoparticles (Al_2O_3-NPs) from recycled packaging cans and their incorporation into polymer coatings as active packaging materials with antimicrobial properties present significant advancements for the packaging industry. These innovative materials offer an efficient approach to enhancing food safety, prolonging shelf life and minimizing waste. With ongoing progress in nanotechnology and polymer science, the application of Al_2O_3-NPs in active packaging is anticipated to expand, contributing to the development of more sustainable, high-performance packaging solutions in the future.

Data Availability Statement

The data that support the findings of this study are available from the corresponding author upon reasonable request.

References

1. S. Ibrahim, H. Elsayed, and M. Hasanin, "Correction to: Biodegradable, Antimicrobial and Antioxidant Biofilm for Active Packaging Based on Extracted Gelatin and Lignocelluloses Biowastes (Journal of Polymers and the Environment, (2020))," *Journal of Polymers and the Environment* 29 (2020): 483–490, https://doi.org/10.1007/s10924-020-01940-3.

2. B. W. Chieng, N. A. Ibrahim, W. M. Z. W. Yunus, and M. Z. Hussein, "Plasticized Poly(lactic acid) With Low Molecular Weight Poly(ethylene glycol): Mechanical, Thermal, and Morphology Properties," *Journal of Applied Polymer Science* 130 (2013): 4576–4580, https://doi.org/10.1002/app.39742.

3. S. Ibrahim and K. M. El-Khawas, "Development of Eco-Environmental Nano-Emulsified Active Coated Packaging Material," *Journal of King Saud University, Science* 31 (2019): 1485–1490, https://doi.org/10.1016/j.jksus.2019.09.010.

4. I. Ahmed, H. Lin, L. Zou, et al., "A Comprehensive Review on the Application of Active Packaging Technologies to Muscle Foods," *Food Control* 82 (2017): 163–178, https://doi.org/10.1016/J.FOODCONT.2017.06.009.

5. S. Ibrahim, H. El Saied, and M. Hasanin, "Active Paper Packaging Material Based on Antimicrobial Conjugated Nano-Polymer/Amino Acid as Edible Coating," *Journal of King Saud University, Science* 31 (2019): 1095–1102, https://doi.org/10.1016/j.jksus.2018.10.007.

6. S. Ghotekar, "Plant Extract Mediated Biosynthesis of Al_2O_3 Nanoparticles—A Review on Plant Parts Involved, Characterization and Applications," *Nanochemistry Research* 4 (2019): 163–169, https://doi.org/10.22036/ncr.2019.02.008.

7. L. Önnby, V. Pakade, B. Mattiasson, and H. Kirsebom, "Polymer Composite Adsorbents Using Particles of Molecularly Imprinted Polymers or Aluminium Oxide Nanoparticles for Treatment of Arsenic Contaminated Waters," *Water Research* 46 (2012): 4111–4120, https://doi.org/10.1016/J.WATRES.2012.05.028.

8. A. H. Gharbi, S. E. Laouini, H. Hemmami, et al., "Eco-Friendly Synthesis of Al_2O_3 Nanoparticles: Comprehensive Characterization Properties, Mechanics, and Photocatalytic Dye Adsorption Study," *Coatings* 14 (2024): 848–862.

9. M. B. Gawande, A. Goswami, F.-X. Felpin, et al., "Cu and Cu-Based Nanoparticles: Synthesis and Applications in Catalysis," *Chemical Reviews* 116 (2016): 3722–3811, https://doi.org/10.1021/acs.chemrev.5b00482.

10. A. I. Osman, Y. Zhang, M. Farghali, et al., "Synthesis of Green Nanoparticles for Energy, Biomedical, Environmental, Agricultural, and Food Applications: A Review," *Environmental Chemistry Letters* 22 (2024): 841–887, https://doi.org/10.1007/s10311-023-01682-3.

11. S. Kazemi, A. Hosseingholian, S. D. Gohari, et al., "Recent Advances in Green Synthesized Nanoparticles: From Production to Application," *Materials Today Sustainability* 24 (2023): 100500, https://doi.org/10.1016/j.mtsust.2023.100500.

12. L.-R. Lee, Y.-F. Chen, S. Zheng, M. H. Chang, and J. T. Chen, "Upcycling Discarded Aluminum Cans Into Nanoporous Membranes as an Eco-Friendly and Cost-Effective Strategy for Fabricating Polymer Nanoarrays and Self-Cleaning Surfaces," *ACS Applied Nano Materials* 6 (2023): 18558–18570, https://doi.org/10.1021/acsanm.3c04051.

13. A. J. R. Castro, S. P. D. Marques, J. M. Soares, J. M. Filho, G. D. Saraiva, and A. C. Oliveira, "Nanosized Aluminum Derived Oxides Catalysts Prepared With Different Methods for Styrene Production," *Chemical Engineering Journal* 209 (2012): 345–355, https://doi.org/10.1016/J.CEJ.2012.07.094.

14. R. Kumar, G. R. Pulikanti, K. R. Shankar, et al., "Surface Coating and Functionalization of Metal and Metal Oxide Nanoparticles for Biomedical Applications," in *Metal Oxides for Biomedical and Biosensor Applications* (Elsevier, 2022): 205–231, https://doi.org/10.1016/B978-0-12-823033-6.00007-7.

15. K. B. Narayanan, R. Bhaskar, and S. S. Han, "Bacteriophages: Natural Antimicrobial Bioadditives for Food Preservation in Active Packaging," *International Journal of Biological Macromolecules* 276 (2024): 133945, https://doi.org/10.1016/J.IJBIOMAC.2024.133945.

16. A. Adibi, B. M. Trinh, and T. H. Mekonnen, "Recent Progress in Sustainable Barrier Paper Coating for Food Packaging Applications," *Progress in Organic Coatings* 181 (2023): 107566, https://doi.org/10.1016/J.PORGCOAT.2023.107566.

17. S. K. Sahu, V. Boggarapu, and P. S. R. Sreekanth, "Improvements in the Mechanical and Thermal Characteristics of Polymer Matrix Composites Reinforced With Various Nanofillers: A Brief Review," *Materials Today Proceedings* 113 (2023): 1–8, https://doi.org/10.1016/J.MATPR.2023.07.032.

18. J. S. Packialakshmi, J. Kang, A. Jayakumar, S. Park, Y. Chang, and J. T. Kim, "Insights Into the Antibacterial and Antiviral Mechanisms of Metal Oxide Nanoparticles Used in Food Packaging," *Food Packaging and Shelf Life* 40 (2023): 101213, https://doi.org/10.1016/j.fpsl.2023.101213.

19. R. K. Gupta, G. F. A. El, E. A. E. Ali, et al., "Nanotechnology: Current Applications and Future Scope in Food Packaging Systems," *Measurement: Food* 13 (2024): 100131, https://doi.org/10.1016/J.MEAFOO.2023.100131.

20. M. S. de Sousa, A. E. Schlogl, F. R. Estanislau, V. G. L. Souza, J. S. dos Reis Coimbra, and I. J. B. Santos, "Nanotechnology in Packaging for Food Industry: Past, Present, and Future," *Coatings* 13 (2023): 1411–1429, https://doi.org/10.3390/COATINGS13081411.

21. J. O. Adeyemi and O. A. Fawole, "Metal-Based Nanoparticles in Food Packaging and Coating Technologies: A Review," *Biomolecules* 13 (2023): 1092–1119, https://doi.org/10.3390/BIOM13071092.

22. M. Adhar, B. HadjKacem, S. Périno-Issartier, et al., "Thymol-Enriched Extract From *Thymus vulgaris* L Leaves: Green Extraction Processes and Antiaggregant Effects on Human Platelets," *Bioorganic Chemistry* 125 (2022): 105858, https://doi.org/10.1016/J.BIOORG.2022.105858.

23. S. Ibrahim, M. Abdel Rehim, and G. Turky, "Dielectric Study of Polystyrene/Polycaprolactone Composites Prepared by Miniemulsion Polymerization," *Journal of Physics and Chemistry of Solids* 119 (2018): 56–61, https://doi.org/10.1016/J.JPCS.2018.03.030.

24. A. Meawad and S. Ibrahim, "Novel Bifunctional Dispersing Agents From Waste PET Packaging Materials and Interaction With Cement," *Waste Management* 85 (2019): 563–573, https://doi.org/10.1016/J.WASMAN.2019.01.028.

25. X. Cao, F. Nan, W. Fan, et al., "Preparation, Formation Mechanism, and Performance of Nitrocellulose Aqueous Coating Based on the Anti-Solvent Method," *Colloids and Surfaces A: Physicochemical and Engineering Aspects* 684 (2024): 133214, https://doi.org/10.1016/J.COLSURFA.2024.133214.

26. P. Li, S. Wang, and S. Zhou, "Film Formation Behavior and Mechanical Properties of one-Component Waterborne Crosslinkable Polysiloxane/Fumed Silica Nanocomposite Coatings," *Progress in Organic Coatings* 147 (2020): 105870, https://doi.org/10.1016/J.PORGCOAT.2020.105870.

27. J. L. Hall, A. Pérez, E. L. Kynaston, C. Lindsay, and J. L. Keddie, "Effects of Environmental Conditions on the Micro-Mechanical Properties

of Formulated Waterborne Coatings," *Progress in Organic Coatings* 163 (2022): 106657, https://doi.org/10.1016/J.PORGCOAT.2021.106657.

28. S. Ibrahim, A. Labeeb, A. F. Mabied, et al., "Synthesis of Super-Hydrophobic Polymer Nanocomposites as a Smart Self-Cleaning Coating Films," *Polymer Composites* 38 (2017): E147–E156, https://doi.org/10.1002/pc.24023.

29. B. Dziejarski, D. F. Hernández-Barreto, J. C. Moreno-Piraján, et al., "Upgrading Recovered Carbon Black (rCB) From Industrial-Scale End-of-Life Tires (ELTs) Pyrolysis to Activated Carbons: Material Characterization and CO_2 Capture Abilities," *Environmental Research* 247 (2024): 118169, https://doi.org/10.1016/J.ENVRES.2024.118169.

30. J. Vandervoort and A. Ludwig, "Preparation and Evaluation of Drug-Loaded Gelatin Nanoparticles for Topical Ophthalmic Use," *European Journal of Pharmaceutics and Biopharmaceutics* 57 (2004): 251–261, https://doi.org/10.1016/S0939-6411(03)00187-5.

31. M. Vaca Guerra, Y. M. Harshe, L. Fries, S. Rothberg, S. Palzer, and S. Heinrich, "Influence of Particle Size Distribution on Espresso Extraction via Packed Bed Compression," *Journal of Food Engineering* 340 (2023): 111301, https://doi.org/10.1016/J.JFOODENG.2022.111301.

32. A. D'Elia, B. Alfakes, A. Alkhazaleh, et al., "Characterization of a Transmon Qubit in a 3D Cavity for Quantum Machine Learning and Photon Counting," *Applied Sciences* 14 (2024): 1478–1498, https://doi.org/10.3390/app14041478.

33. P. A. Prashanth, R. S. Raveendra, R. Hari Krishna, et al., "Synthesis, Characterizations, Antibacterial and Photoluminescence Studies of Solution Combustion-Derived α-Al_2O_3 Nanoparticles," *Journal of Asian Ceramic Societies* 3 (2015): 345–351, https://doi.org/10.1016/j.jascer.2015.07.001.

34. A. Henning, J. D. Bartl, A. Zeidler, et al., "Aluminum Oxide at the Monolayer Limit via Oxidant-Free Plasma-Assisted Atomic Layer Deposition on GaN," *Advanced Functional Materials* 31 (2021): 2101441, https://doi.org/10.1002/adfm.202101441.

35. K. R. Overdeep, C. J. Ridge, Y. Xin, T. N. Jensen, S. L. Anderson, and C. M. Lindsay, "Oxidation of Aluminum Particles From 1 to 10 nm in Diameter: The Transition From Clusters to Nanoparticles," *Journal of Physical Chemistry C* 123 (2019): 23721–23731, https://doi.org/10.1021/acs.jpcc.9b05564.

36. S. Xiong and D. Liang, "High-Temperature Diffusion Behavior, Wear-Resistance and Corrosion-Resistance Properties of Al_2O_3, MoS_2, and ZnO Nanoparticles on Copper Surfaces," *Surfaces and Interfaces* 58 (2025): 105840, https://doi.org/10.1016/J.SURFIN.2025.105840.

37. A. Aghanejad, S. F. Bonab, M. Sepehri, et al., "A Review on Targeting Tumor Microenvironment: The Main Paradigm Shift in the mAb-Based Immunotherapy of Solid Tumors," *International Journal of Biological Macromolecules* 207 (2022): 592–610, https://doi.org/10.1016/j.ijbiomac.2022.03.057.

38. D. Wang, X. Wang, S. Zhou, et al., "Radish Residue Carbon Dots-Based Novel Starch/Chitosan Film With High Antioxidant, Biocompatibility, and Antibacterial Activities for Salmon Fillets' Active Packaging," *International Journal of Biological Macromolecules* 273 (2024): 133107, https://doi.org/10.1016/J.IJBIOMAC.2024.133107.

39. S. Ibrahim, H. Fahmy, and S. Salah, "Application of Interactive and Intelligent Packaging for Fresh Fish Shelf-Life Monitoring," *Frontiers in Nutrition* 8 (2021): 1–8, https://doi.org/10.3389/fnut.2021.677884.